Proceedings of GT2006
ASME Turbo Expo 2006: Power for Land, Sea and Air
May 8-11, 2006, Barcelona, Spain

GT2006-91237

THE USE OF HIGH BLOCKAGE RIBS TO ENHANCE HEAT TRANSFER COEFFICIENT DISTRIBUTIONS IN A MODEL OF AN INTEGRALLY CAST COOLING MANIFOLD

Ioannis Ieronymidis, David R.H. Gillespie and Peter T. Ireland
Department of Engineering Science, University of Oxford
Parks Road, Oxford OX1 3PJ, United Kingdom
Fax: +44 1865 288756
E-Mail: ioannis.ieronymidis@eng.ox.ac.uk

Robert Kingston
Rolls-Royce plc.
PO Box 3, Filton, Bristol BS34 7QE
United Kingdom
E-Mail: robert.kingston@rolls-royce.com

ABSTRACT

In this paper detailed experimental measurements and computational predictions of heat transfer coefficient distributions in a large scale perspex model of a novel integrally cast blade cooling geometry are reported. In a gas turbine blade, the cooling passage investigated is integrally cast into the blade wall, providing good thermal contact with the outer surface of the turbine blade. Flow enters the racetrack passage through the root of the blade and exits to a central plenum through a series of nineteen transfer holes equally spaced in a staggered arrangement across the span of the blade. The Reynolds number changes continuously along the passage length because of the continuous ejection of fluid through a series of 19 transfer holes to the plenum. The smooth passage surface opposite is in closest proximity to the external surface, and this investigation has characterised the heat transfer coefficient on this surface at a range of engine representative inlet Reynolds numbers using a hybrid transient liquid crystal technique. The ability of three different rib configurations to enhance the heat transfer on this surface was also determined. Because the passage at engine scale is necessarily small, the rib height in all cases was 32.5% of the passage height. As the entire passage wetted surface is able to contribute to the blade cooling, and knowledge of the heat transfer coefficient distribution on the holed surfaces is crucial to prediction of blade life, a commercial CFD package, Fluent, was used to predict the heat transfer coefficient distributions on the holed surface, where there was no optical access during these tests. This also allowed investigation of additional rib configurations, and comparison of the pressure penalty associated with each design. The study showed that the turbulator configuration used allows the position and maximum level of heat transfer coefficient enhancement to be chosen by the engine designer. For the configurations tested heat transfer coefficient enhancement of up to 32% and 51% could be achieved on the holed surface and the ribbed surface respectively. For minimum additional pressure drop 45° ribs should be used.

Key words: heat transfer, ribs, CFD

INTRODUCTION

Effective cooling inside gas turbine blade passages allows higher turbine inlet temperatures that generally result in better power output from the engine or improved specific fuel consumption. For this purpose, several strategies including impingement cooling, film cooling and ribbed serpentine passage cooling have been employed in recent years to maximize the heat transferred from the blade to the coolant. The aim is to obtain the required metal temperature using the lowest possible coolant mass flow rate at the lowest possible driving pressure. In the vast majority of cooling configurations, turbulators are used in serpentine passages to enhance turbulence and flow swirl resulting in higher heat transfer coefficients. Most previous research has only been able to determine the heat transfer performance on the surfaces between the turbulators and subsequently there are very little data characterising the heat transfer performance of the actual turbulators. These are not only the region of highest heat transfer, but may also constitute a major proportion of the exposed passage surface area, particularly in the case of high blockage ribs. In this study, rib large blockage turbulators are used in a wall cooling passage, connected to central plena through a series of transfer holes. The turbulators are placed on the wall in closest proximity to the blade

external surface. The blockage ratio (e/D_h) and pitch-to-height ratio (p/e) of the ribs is 21 % and 8.7 respectively. The rib pitch is equal to the hole pitch. It has been shown that, even in the absence of ribs, the heat transfer coefficient distribution on the holed surface is significantly enhanced over a smooth passage by the stripping and restarting of the boundary layer in the region downstream of the hole (Ieronymidis et al. [1]). The use of rib turbulators allows the designer to enhance the heat transfer on the ribbed wall. The choice of which ribbed configuration is the most suitable depends on the particular cooling requirements and the desired passage static pressure drop. This study experimentally and computationally has characterised the heat transfer and pressure drop coefficients for a number of candidate rib geometries. Heat transfer to both the major passage walls is characterised, and the level of heat transfer coefficient predicted by the CFD study is compared to experimental results.

Ribs and similar turbulators have been the subject of much previous study. Early work by Berger et al. [2] investigated the effect of flow over square ribs in a circular pipe and measured heat transfer coefficients on the ribs as well as the walled surfaces between them. Using a blockage ratio of 3.4 % whilst varying the rib pitch-to-height ratio from 3 to 10 over a range of Reynolds numbers between 10,000 and 25,000 they showed enhancement in total heat transfer on the ribbed surfaces, of 4.4 to 5.2. Metzger et al. [3] examined the contribution of the rib heat transfer to the overall heat transfer of a rib-roughened wall with variations in rib angle of attack and pitch. At a blockage ratio of 14%, more representative of a gas turbine passage, they observed significant *htc* enhancement, mainly dependent on the rib pitch-to-height spacing, with very little effect from the rib angle.

Taslim and Wadsworth [4] tested 13 rib geometries with 90° ribs mounted on two opposite walls. They concluded that the highest rib heat transfer coefficient occurred when the rib pitch-to-height ratio was 8.5, and heat transfer coefficients on ribs in the most upstream position were lower than those for mid-channel ribs, suggesting that secondary flow fields take 3-4 rib pitches to become fully developed. In a later study Korotky and Taslim [5] showed the importance of the rounded edges of ribs in determining the size of the flow separation downstream of the rib.

The need for accurate resolution of small flow features has limited modelling of ribbed passages using CFD. Hermanson et al. [6] investigated the validity of a number of turbulence models in simulating a ribbed passage with a 10 % blockage ratio and varying angles of rib inclination. He concluded that the turbulence models used ($k-\varepsilon$ with wall functions and 2 layer, V2F) accurately predict the pressure losses due to the ribs and the qualitative heat transfer distribution on the ribbed wall. However, only the V2F model accurately reproduced the absolute heat flux levels at all inclination angles. Heat transfer levels on the ribs were found to be 15 to 50 % greater than on the ribbed wall.

Hwang et al. [7] studied the heat transfer in a radially rotating four-pass serpentine channel with staggered half-V rib turbulators. They concluded that ribs placed 120° against the main flow in the second and fourth passages has beneficial effects in local heat transfer, especially in the region of the first turn, the second passage and the second turn. Tsang at al. [8] studied the effects of high blockage turbulators in gas turbine cooling passages and tested 13 rib geometries with blockage ratios of 16 and 30 % and rib angles of 90°, 45° and 60°. They used several configurations including staggered ribs, in-line ribs, crossed ribs and combinations of these. He concluded that ribbed walls have the highest *Nu* level because of the larger heat transfer surface area, and the locally enhanced *htc* levels. The smooth walls on either side of the passage have similar heat transfer coefficient levels in most configurations, despite the different *local* patterns on each wall. In all cases this level is significantly higher than in the equivalent smooth square duct.

NOMENCLATURE

A	cross sectional area (m^2)
a,b	heat transfer parameters
C_p	specific heat capacity at constant pressure (J/kgK)
D_h	hydraulic diameter of passage = $4\,A\,/\,P$ (m)
d	hole diameter or depth of material on which liquid crystals are sprayed on (m)
e	height of the turbulator (m)
h, *htc*	heat transfer coefficient (W/m^2K)
k	thermal conductivity (W/m K)
l_c	coating thickness (m)
l_{rib}	length of rib (m)
Nu	Nusselt number = $h\,d\,/\,k$
P	perimeter of cross section of passage (m)
p	pressure (Pa) or turbulator pitch (m) in p/e
Re	Reynolds number = $\rho\,u\,d\,/\,\mu$
SR	suction ratio, $u_{hole}/u_{passage}$
s	wall thickness of hollow copper turbulator (m)
T	temperature (K)
t	running time of heat transfer experiments (s)
u	velocity (m/s)
x	distance (m)
y	distance (m) or distance of the centroid of the cell to the wall in CFD (m)

Greek

μ	dynamic viscosity (Ns/m^2)
ρ	density (kg/m^3)

Abbreviations

TC	thermocouple
TLC	thermochromic liquid crystals
VHR	velocity head ratio = $(\,p_{0i} - p_{se}\,)/(\,p_{0i} - p_{si}\,)$

Subscripts

0	total
e	exit
g	gas
i	inlet
s	static
w	wall
c	crystal

EXPERIMENTAL APPARATUS

A large scale rig of a single cooling passage was constructed. The working section was built from perspex which ensured good optical access and low thermal diffusivity. Figure 1 shows a schematic of the rig. Figure 2 describes in detail the working section of the rig. The model is approximately 20× engine scale. This scale was chosen to allow both the Reynolds number and Suction Ratio *SR*, to be matched to engine conditions. It was not necessary to match the Mach number as it was less than 0.2 over the full range of engine representative conditions, see Andrews and Mkpadi [9]. The air intake is atmospheric. Hole centres are located $y/d = \pm 1.77$ from the passage centreline; the hole pitch is $x/d = 6.54d$ along the passage axis. The

first hole is located at x/d = 13.08, and the total passage length is x/d = 147.5. The distance between the holed surface and the flat or ribbed surface was 2.31d.

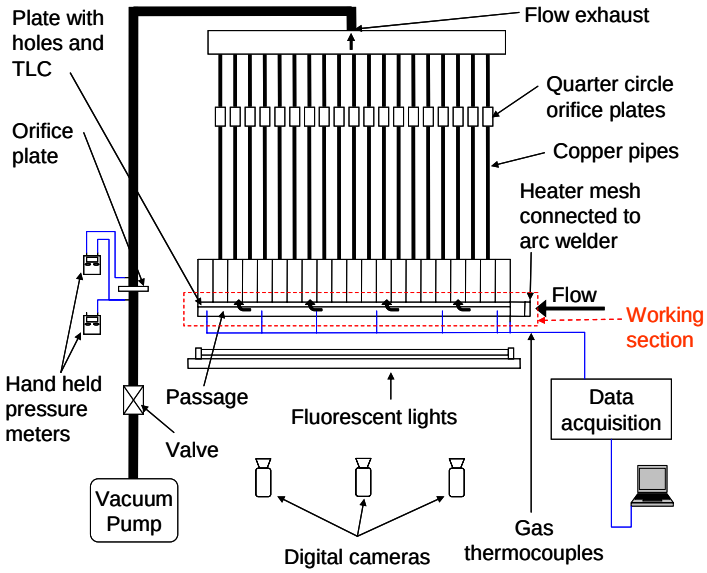

Figure 1 – Schematic of experimental setup (not to scale)

The holes are orientated at 90° to the oncoming flow. The length of the holes was 1.5d. A 45° casting representative chamfer, 0.125d deep is included on the passage side of the holes. Flow entering the passage is bled through these holes resulting in a reduction of the crossflow passage velocity with distance from the inlet. The passage has a characteristic racetrack shape in cross-section. The flow through each hole in the manifold was separately metered and additionally the total mass flow rate was measured at the rig exit using orifice meters designed in accordance with BS1042. Temperature data were obtained using T-type thermocouples and thermochormic liquid crystal coatings. The colour change of the coated surfaces was monitored using a number of digital video cameras. The gas temperature transient required for heat transfer tests was produced by a planar heater mesh located at the passage inlet.

Note that the uncertainty in the measured gas temperature takes account of possible effects of radiation from the mesh heater at all thermocouple locations along the passage. Although the mesh heater is in close proximity to the first thermocouple, because of the high convective efficiency of the heater (0.3 – 0.5 dependent on flow velocity), the temperature of the heater wires lies between 100ºC and 160ºC. Thus even at the lowest flow rate the first thermocouple will merely over read the inlet gas temperature by ~0.01°C. No correction was applied to the reading to take account of this.

The area over which the heat transfer coefficient distribution was determined is indicated in Figure 3. This is the wall on which the rib turbulators were positioned. A hybrid transient liquid crystal technique was used to obtain local surface heat transfer coefficient distributions on the wall, and bulk heat transfer coefficients on the ribs. Hence the surface shown was first sprayed with a 10 – 30 µm thick liquid crystal coating, and subsequently with black ink to improve the visibility of the liquid crystal colour play. The various rib configurations tested are shown in Figure 4.

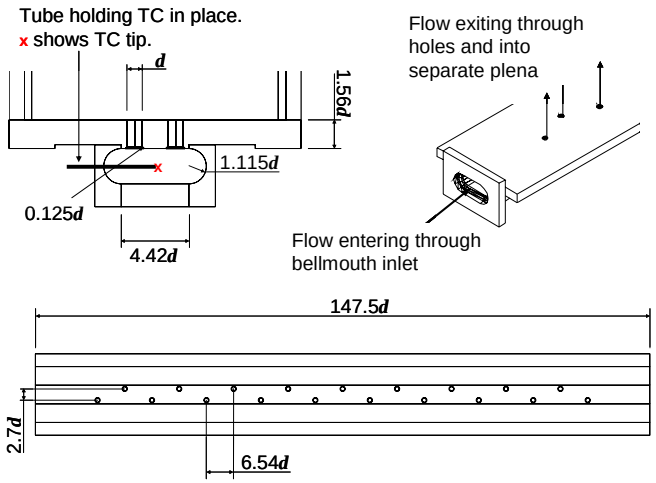

Figure 2 – Detailed description of working section geometry

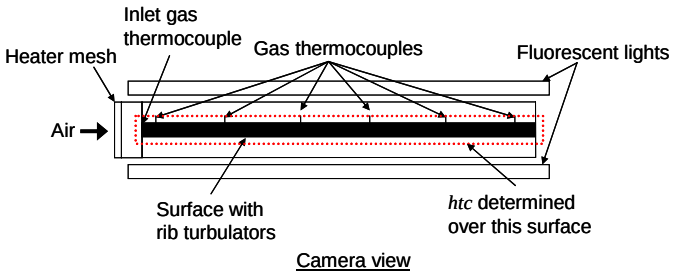

Figure 3 – Camera and lighting arrangement for passage *htc* experiments (not to scale)

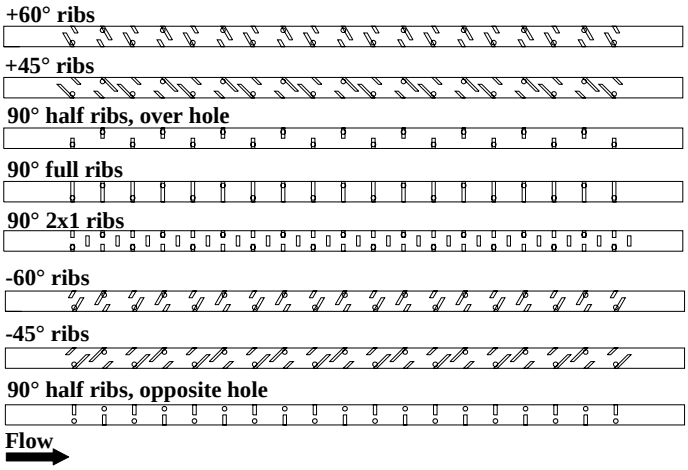

Figure 4 – Rib configurations tested using experimental techniques and CFD

Note that the holes shown in Figure 4 lie on the opposing wall of the channel and are drawn for reference purposes only. The +60º, 90º half rib-over hole and 90º full rib configurations were tested experimentally. The remaining rib configurations were modelled using CFD simulations, allowing a qualitative comparison to the experimentally measured data. All rib turbulators tested were made from 0.75d × 0.75d square

sectioned hollow copper tubes, sealed at each end by thin sheets of plastic tape. They were attached to the liquid crystal and ink coated surface using a thin layer of acrylic binder and a locating screw. The rib pitch, measured from the rib base, was constant, and equal to the hole pitch. In the case of the 60º and 45º ribs configurations staggered ribs were used that were not equal in size, one rib spanning 1/3 of the passage width and the other 2/3. The larger rib was placed so that it was opposite and just upstream of each transfer hole. It was hoped that this would ensure that the rib would interact strongly with flow being accelerated into each hole.

HYBRID TRANSIENT HEAT TRANSFER TECHNIQUE

The transient heat transfer technique employing liquid crystals is well established and its method of implementation in these experiments is fully described in Abu Talib et al. [10]. The heat transfer coefficients obtained are based on the local centreline passage temperature determined by interpolation between measurements at 7 locations along the cooling passage. For the test surface to behave as a semi-infinite solid, the time taken for the full liquid crystal colour play to occur must be relatively short compared to the time taken for the thermal pulse to travel through the wall of the test rig and begin dissipating heat to the surrounding environment. Schultz and Jones [11] showed that the time, *t*, taken for the thermal pulse to travel across a wall of depth, *d*, is calculated by

$$t = \frac{d^2}{16\alpha} \tag{1}$$

where α is the thermal diffusivity of the material and has a value of 1.08×10^{-7} m^2/s for perspex. With a perspex plate of depth 0.0125 m, the maximum test time was thus calculated to be 90.42 s.

Lack of optical access means that it is impossible to obtain full local heat transfer coefficient data on the ribbed surfaces. However, these are area of high *htc*, and it is insufficient to report merely the value on top of the rib. Therefore, the average heat transfer coefficient on the rib based on the projected area of the rib in the passage was determined using the analysis technique developed for grain roughness heat transfer measurements by Wang [12]. The roughness surface temperature rise for a step change in gas temperature is related to the effective heat transfer coefficient, *h*, and the coating capacity, β_c defined as:

$$\beta_c = \rho_c c_{p_c} l_c \left(1 - \frac{h l_c}{2k_c}\right), \text{ by} \tag{2}$$

$$\frac{T_w(t) - T_i}{T_g - T_i} = 1 + h\left[\frac{\exp(\alpha^2 t)erfc(\alpha\sqrt{t})}{\beta_c a(a-b)} - \frac{\exp(b^2 t)erfc(b\sqrt{t})}{\beta_c b(b-a)}\right], \tag{3}$$

where

$$a = \frac{\sqrt{\rho c_p k}}{2\beta_c}\left(1 + \sqrt{1 - \frac{4\beta_c h}{\rho c_p k}}\right), \text{and } b = \frac{\sqrt{\rho c_p k}}{2\beta_c}\left(1 - \sqrt{1 - \frac{4\beta_c h}{\rho c_p k}}\right), \tag{4,5}$$

Here l_c represents the equivalent coating thickness of the turbulator. This is calculated from the volume of the turbulator divided by its footprint area, $l_c = 4s(1 - s/e)$ (6). Copper was selected because it has a high thermal conductivity and during the transient heat transfer experiment it can be considered isothermal. Thus, the temperature observed at the liquid crystal - copper interface is the temperature of the turbulator. A hollow rib was used to ensure that the colour change of the liquid crystal under the rib occurs during the prescribed maximum test time.

COMPUTATIONAL MODEL

CFD simulations were carried out using the commercial package Fluent. The full experimental geometry was modelled. In order to be able to satisfy the required condition that $y^+ \leq 1$ for all inlet Reynolds numbers a 15 layer boundary layer mesh was used in the cooling passage, however computational limitations meant that no boundary layer mesh was applied to the surfaces of the ribs. The remaining volume was meshed using tetrahedral elements resulting in a hybrid mesh. Sizing functions were used to control the cell growth inside the holes. The total number of cells was approximately 2.3 million. Incompressible flow was assumed. Figure 5 shows one of the grids used in the simulations. The boundary layer mesh can be seen in the inset picture. The cylindrical features on top of the transfer holes act as individual exit plena for each transfer hole. This allows mass flow rate or pressure distributions at the hole exits to be specified.

Thermal and mass flow rate boundary conditions were prescribed to match experimental running conditions without ribs, as pressure measurements on the experimental rig indicated that the mass flow rate distribution through the transfer holes was not significantly affected by the presence of the ribs (within $\pm$ 2.3 % of the smooth wall case).

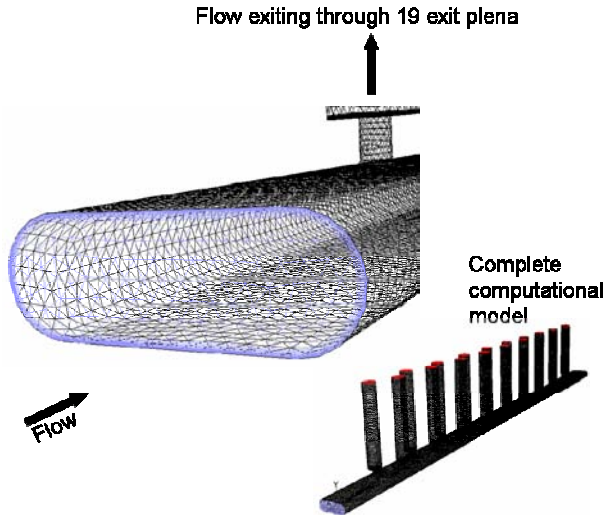

Figure 5 – Geometry and grid in CFD

Steady CFD simulations were carried out using the realisable $k-\varepsilon$ turbulence model with enhanced wall treatment. This has been shown to provide reliable predictions for bounded duct flows (Fluent [13]). Heat transfer coefficients based on local passage conditions were calculated from the local surface heat flux and local passage centreline temperature data. These could then be directly compared to measured experimental data.

RESULTS

Experimental heat transfer distributions

Figure 6 shows the *htc* distributions obtained for the three rib configurations and for a smooth wall, tested at an inlet Reynolds number of 45596. All *htc* values reported are based on the local passage centreline temperature. Local heat transfer coefficient

distributions are shown between ribs and a single averaged value on each rib – this is based on the projected rib area (i.e. the averaged local *htc* × 3). At the end of the passage, where there is no crystal activity the heat transfer coefficients are undefined. The *htc* scale is chosen to allow visualisation of *htc* patterns. The rib *htc* values are, therefore, out of scale and are presented in Figure 9. The discharge coefficient distribution for the holes and local passage Reynolds numbers are presented in Figure 7 for the smooth wall case and Re_{inlet} = 45596. Looking at the results it is clear that the section of the passage upstream of the first hole behaves similarly for all configurations, including the smooth walled passage. The level depends only on the inlet Reynolds number.

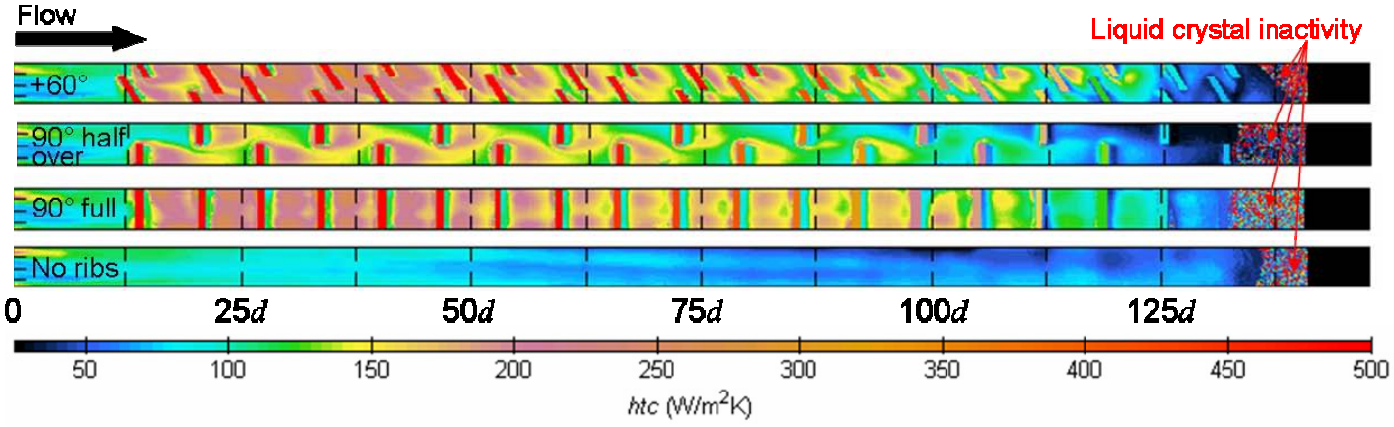

Figure 6 – Experimental *htc* distributions for Re_{inlet} = 45596

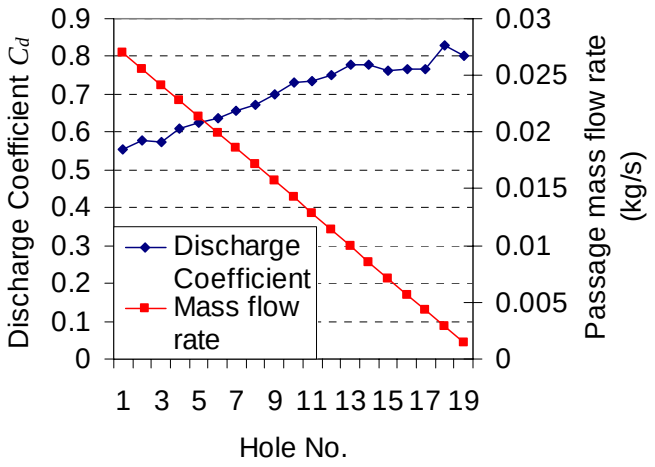

Figure 7 – Passage $\dot{m}$ and C_d for Re_{inlet} = 45596

The flow is modified for all configurations by the presence of the first hole and rib, and behaviour is steady and repeating by third rib pitch. Note that, as expected the heat transfer coefficient drops along the entire length of the passage as flow is ejected through the transfer holes. In the case with no ribs in the passage, it is evident that the position of the first hole (which lies 13.08*d* from the inlet on the lower side of the passage) biases the flow along the entire passage length, creating a streak of high heat transfer coefficient towards the lower side of this surface. The 90º half ribs (over hole) configuration also shows this behaviour, although clearly the level of *htc* is greatly increased. The +60º ribs bias high heat transfer towards the top side of the passage. When the orientation of the 60º ribs is changed to -60º this biasing is also reversed. The 90º full ribs configuration shows the most symmetrical levels of heat transfer coefficient: here the blockage presented by the ribs dominates the flow field, and the secondary flows previously induced by flow ejection are suppressed. At Re_{inlet} = 21667 and Re_{inlet} = 69959 the pattern of heat transfer coefficients seen are very similar, though the levels are sensibly lower and higher than in Figure 6.

Pitch-wise averaged results

The pitch-wise averaged heat transfer coefficients on each rib repeat, and the surface between the ribs at each of the Reynolds numbers tested is shown in Figure 8 – Figure 10. It is clear that for all inlet Reynolds number tested, the +60º ribs configuration has the best performance. Maximum enhancement on the ribbed surface is obtained for the first 7 holes, after which it drops steadily along the passage. There is also considerable *htc* enhancement in the passage between the ribs for all the configurations tested. This is most pronounced near the passage entrance, and the enhancement is seen to drop sharply after the 13th rib repeat. *Htc* levels are comparable to the smooth wall case over the last 4 hole pitches. For the first seven hole pitches the 90º full ribs have higher *htc* levels than the 90º half ribs, after which *htc* levels on the ribs become comparable, but considerable additional enhancement is still seen on the passage surface for the full ribs.

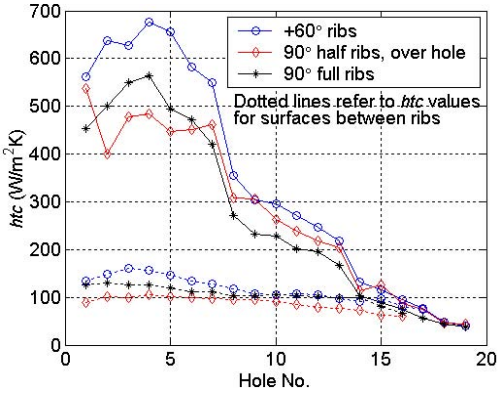

Figure 8 – Rib *htc* for Re_{inlet} = 21667

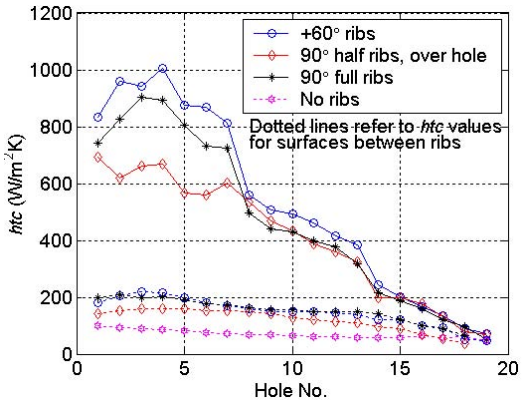

Figure 9 – Rib *htc* for Re_{inlet} = 45596

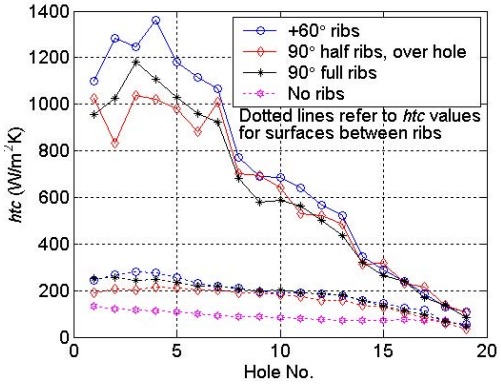

Figure 10 – Rib *htc* for Re_{inlet} = 69959

Heat transfer coefficient values for the surfaces between the ribs

A total, area-weighted, *htc* average for the experimental rib configurations, including the ribs and the surface between the ribs is shown in Figure 11 – Figure 13. At Re_{inlet} = 69959, the +60º ribs configuration gives an average increase of 62 % compared to the case with no ribs. The corresponding value for the 90º full ribs configuration is 58 %. For an inlet Reynolds number of 45596 the values are slightly lower: 58 % and 59 % respectively.

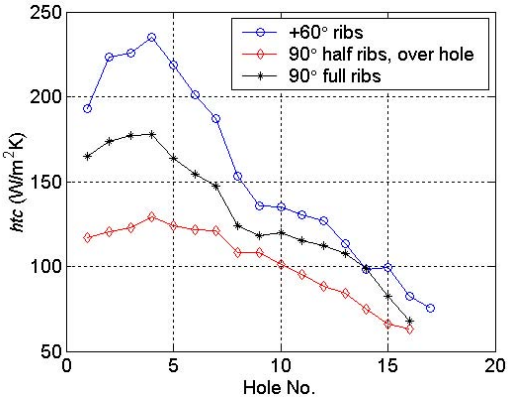

Figure 11 – Total average *htc* for experimental rib configurations for Re_{inlet} = 21667

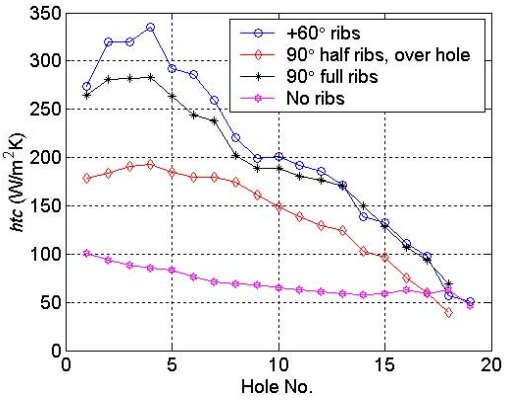

Figure 12 – Total average *htc* for experimental rib configurations for Re_{inlet} = 45596

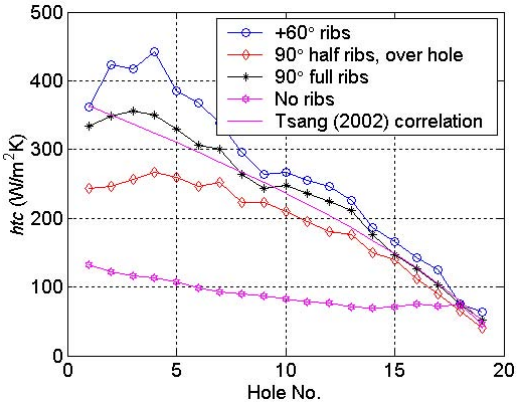

Figure 13 – Total average *htc* for experimental rib configurations for Re_{inlet} = 69959

Figure 13 includes a correlation for 30% e/D_h, +60º [1x1] in-line, parallel ribs of equal size on two opposite walls by Tsang [14]. Although the passage aspect ratio is quite different, and there is no flow extraction the correlation shows good agreement with the current experimental data at the start and towards the end of the passage. The higher level of *htc* between holes 2 and 9 may be attributed to the interaction between the ribbed passage and the boundary layer stripping caused by fluid extraction.

It is evident that the difference in the performance between the three different rib configurations tested for the surfaces between the turbulators becomes smaller as the inlet Reynolds number increases. Overall the +60º ribs configuration displays the highest *htc*, followed closely by the 90º full ribs configuration with the 90º half rib, over hole configuration providing the least enhancement. The pressure drop associated with these configurations is reported below.

Overall heat transfer performance

The system thermal performance has been calculated for the experimentally investigated rib configurations for comparison to other existing cooling designs – particularly low blockage ribs which are widely used in serpentine passages. The ratio of average Nusselt number in the passage to the Nusselt number derived from the Dittus-Boelter correlation is used as a measure of the required heat transfer. The thermal efficiency is defined as this Nusselt number enhancement, divided by the ratio of the friction factor in the passage to the friction factor calculated for a smooth channel with the same distribution of

mass flow rate (after the friction factor correlation of Blasius, see Figure 27). Figure 14 shows these data. Of the configurations experimentally tested, the 60° rib configuration has the best performance (highest position on the y-axis for a given position on the x-axis). Sensibly, the thermal efficiency of the cooling passage reduces as the inlet Reynolds number is increased (marked beside each data point). It is also apparent that in general the low blockage ribs shown have a greater thermal efficiency than the high blockage ribs tested. It is notable that where thermal performance and efficiency coincide between low and high blockage configurations, the high blockage case is running at a reduced inlet Reynolds number. In some cases however (60°, Re_{inlet} = 21667) the high blockage rib allows the thermal performance to increase, while the low Reynolds number is responsible for maintaining a high thermal efficiency. Experimental data from other workers presented in the graph was obtained from [4], [5] and [15].

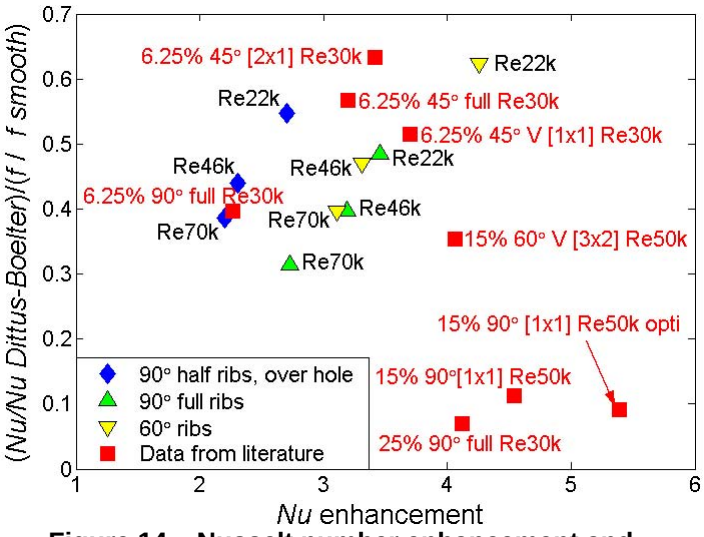

Figure 14 – Nusselt number enhancement and thermal efficiency

Computational heat transfer coefficient results

All CFD simulations reported below were carried out at Re_{inlet} = 69959. Local *htc* distributions were obtained on the ribs, the surfaces between the ribs the holed surfaces on the opposite side of the passage. These data are particularly valuable since experimental results were impossible to obtain in this region as there was no optical access.

Computational local heat transfer coefficient distributions

Figures 15 and 16 show predictions of the local *htc* distributions for the different rib configurations. The heat transfer coefficients are based on the local passage centreline temperature. Comparing the +60° and +45° with the -60° and -45° configurations shows that changing the positioning of the ribs has a profound effect on which side of the passage – top or bottom – has higher average heat transfer coefficients. For the 90º half ribs configurations it is apparent that placing the ribs offset from the hole position on the other side of the passage gives a higher *htc* than placing them over the holes. The effect is similar for the surfaces between the holes. Figure 16 shows the change of shape of the enhancement area downstream of the holes. It is clear that the effect of the angled ribs is to set up a single passage vortex, the direction of rotation of which is, unsurprisingly, changed when the orientation of the ribs is reversed. This effect is most pronounced in the early part of the passage where the velocity head ratio of the flow into the holes has little effect on the flow field.

Heat transfer coefficient values for the ribs

There was no boundary layer mesh attached to the rib surfaces. Therefore results should be considered qualitatively and not quantitatively. Since the ribs were square sectioned there were three rib surfaces in contact with the flow in the passage. To calculate the heat transfer coefficient for each rib and compare it to experimental data, an average value was obtained for each of the three surfaces and then those three values were added together to produce the final *htc* value for the rib. Figure 17 shows *htc* predictions on the rib surfaces.

CFD predicted that the 90º full ribs configuration performed best, with the +60º and the 90º 2x1 ribs configurations following with a very small difference in performance separating them. The authors speculate that the separation is grossly over estimated by the CFD and, therefore, the 90° full ribs slightly outperform the 60° and 45° ribs as the enhancement is primarily attributable to the impingement of flow on the rib upstream surface.

Heat transfer coefficient values for the surfaces between the ribs

Heat transfer coefficient values were averaged over the same areas as used in the presentation of the experimental data to allow direct comparison. Figure 18 shows the averaged *htc* values predicted by the CFD simulation for the surfaces between the ribs. The configurations are identical to those shown in Figure 4. The different orientation of the ribs for the 60º and 45º configurations produce almost identical results, but for the 90º half ribs configurations, placing the ribs opposite the holes instead of over them gives an average increase of 7% in the reported heat transfer coefficient. All the configurations outperform the smooth passage, the 45º configurations enhancing *htc* by the largest amount ~40 %. Figure 19 shows the CFD predicted total area-weighted average *htc* for ribs and the surface between the ribs.

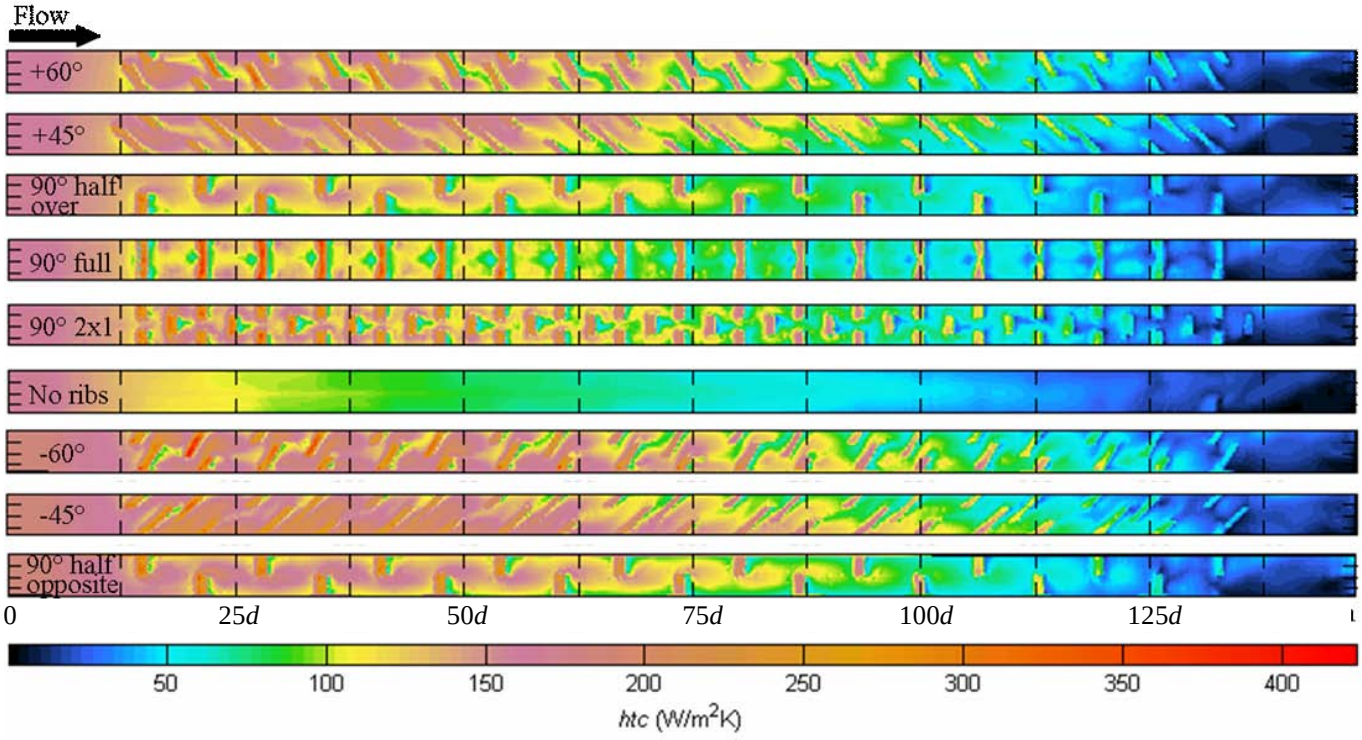

Figure 15 – CFD prediction of *htc* distributions for rib surfaces, Re_{inlet} = 69959

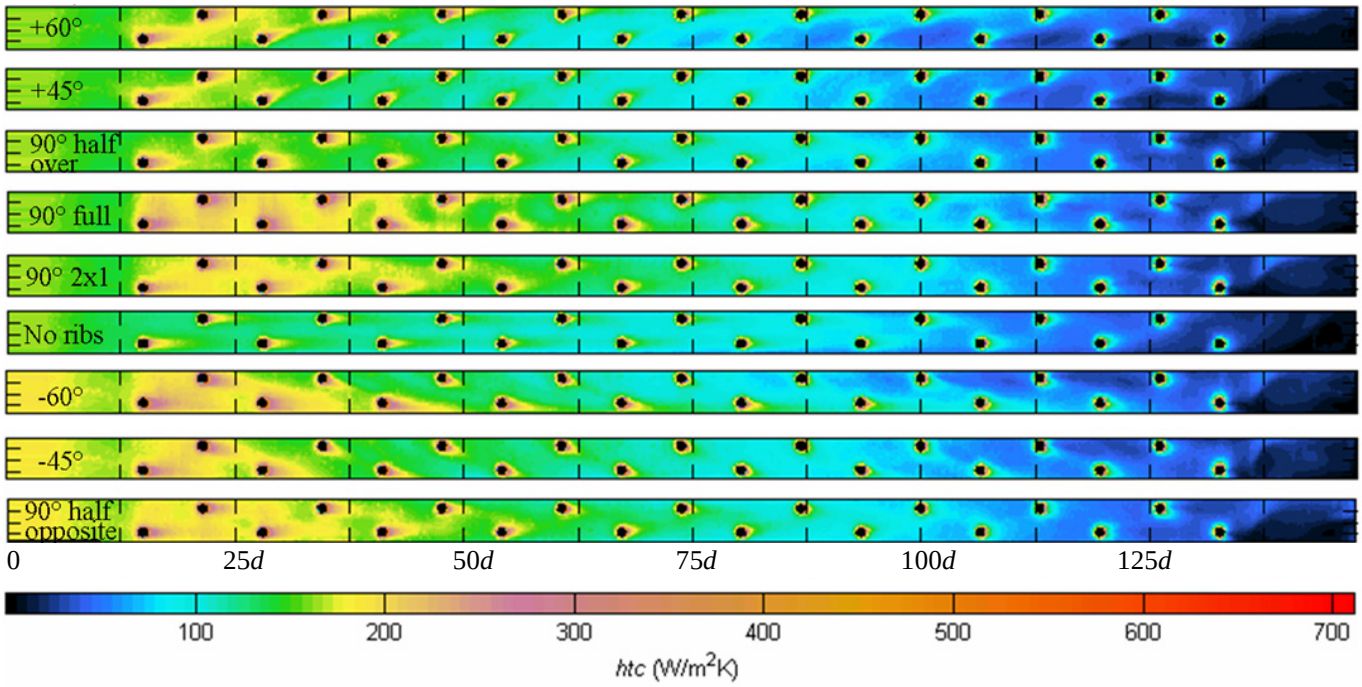

Figure 16 – CFD prediction of *htc* distributions for holed surfaces, Re_{inlet} = 69959

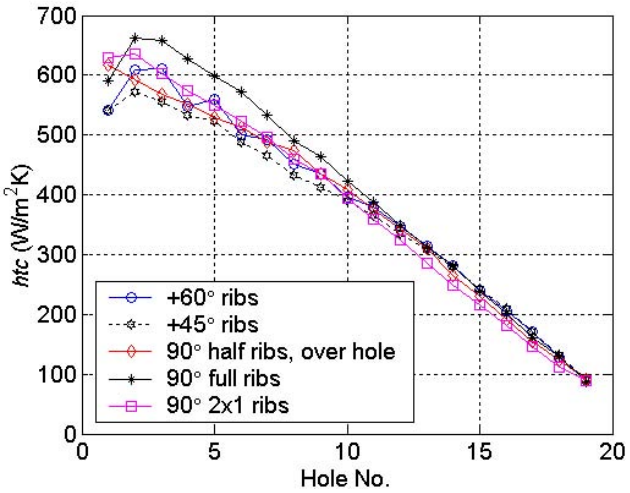

Figure 17 – Average CFD Rib *htc* for Re_{inlet} = 69959

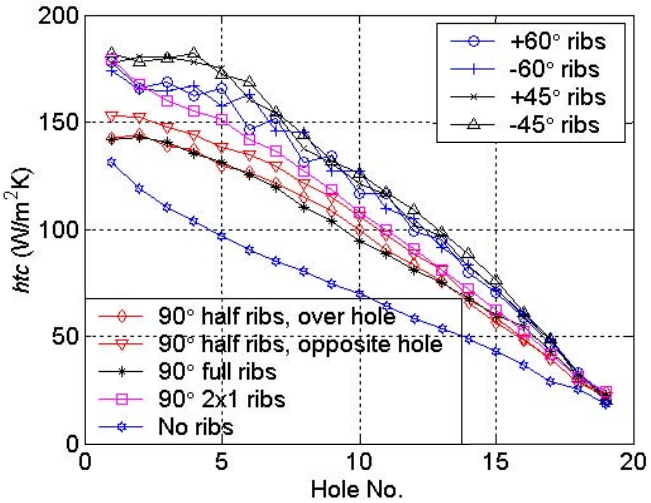

Figure 18 – Average CFD *htc* for surface between ribs, Re_{inlet} = 69959

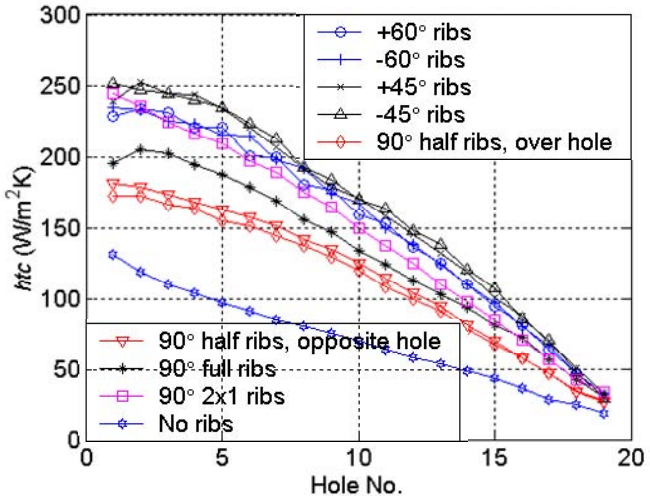

Figure 19 – Total average CFD *htc* for ribs and surface between ribs, Re_{inlet} = 69959

Table 1 shows the total average *htc* increase over the smooth wall case for the predicted CFD results.

Rib configuration	% increase over smooth wall case
+60°	53.3 %
-60°	53.8 %
+45°	56.2 %
-45°	56.3 %
90° half, over hole	36.9 %
90° half, opposite hole	38.7 %
90° full	46.2 %
90° 2x1	50.8 %

Table 1 – Total average *htc* increase over smooth wall case for CFD predictions

Heat transfer coefficient values for the surfaces between the holes

On the opposite side of the passage there is also modification in the level of heat transfer coefficient observed, as shown in Figure 20. Heat transfer coefficient values on the chamfer around the holes were not included in the averaged values for the CFD calculations. However since the chamfer area represents only 0.5 % of the total area between the holes, the results are not significantly affected. Here the heat transfer is enhanced for all configurations near to the entrance of the passage. However, considerable variation in the *htc* enhancement can be seen, with highest enhancement achieved using 90° full ribs followed by 90° 2x1 ribs. Unlike the angled rib configurations which set up a passage vortex, ribs which span the whole passage turn the entire body of the flow in a 2-D sense towards the holed surface, while it continues to move axially along the passage. The flow is locally accelerated in this region, causing the *htc* enhancement. Observing Figure 18 and Figure 20 one can conclude that rib configuration selection can be used to selectively enhance *htc* on either surface.

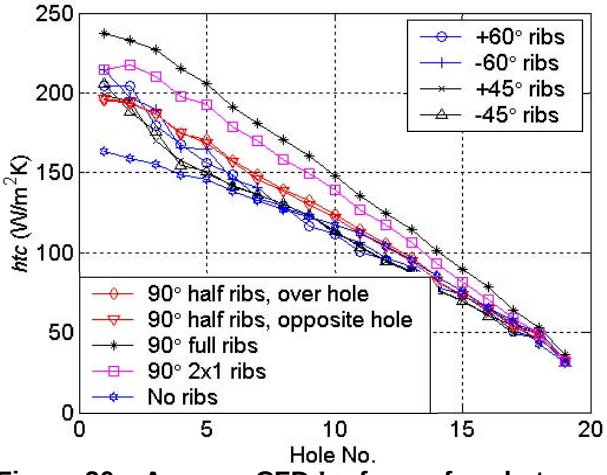

Figure 20 – Average CFD *htc* for surface between holes, Re_{inlet} = 69959

COMPARISON BETWEEN EXPERIMENTAL AND COMPUTATIONAL RESULTS

Average *htc* distributions measured and predicted at an inlet Reynolds number of Re_{inlet} = 69959 are compared in Figure 21 and Figure 22.

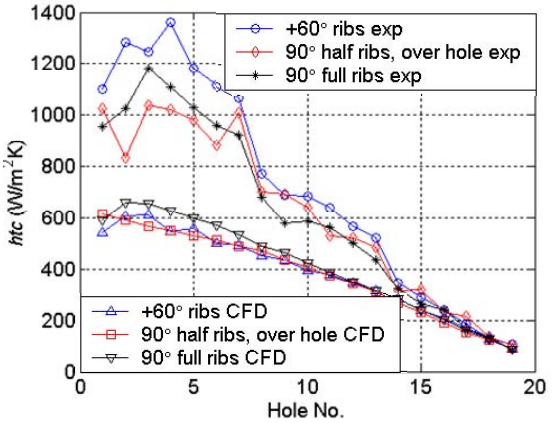

Figure 21 – Rib *htc* comparison between experimental and CFD data

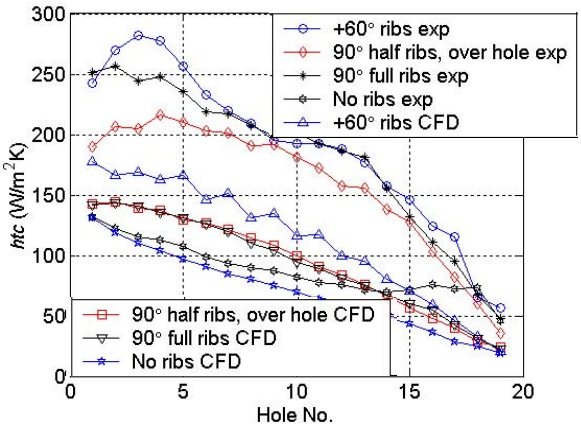

Figure 22 – Surfaces between ribs *htc* comparison between experimental and CFD data

Studying Figure 21 it is clear that the CFD fails to reproduce the experimental results. The level of *htc* for the first seven ribs is underestimated by about a factor of 2. Results improve for the next six holes and become even better for the last two holes but still the general trend that has the 60º configuration outperforming the other configurations is not matched by the computational model. For the surfaces between the ribs (see Figure 22) the 60º configuration performs better in both models, but the other two configurations are not matched. Again CFD underestimates the level of the heat transfer coefficient. Low frequency unsteady effects affect only the last hole of the smooth passage as observed by Ieronymidis et al. [1] during liquid crystal data capture. Hence the difference between experimental and CFD results can be attributed to the deficiency of the turbulence model.

Figures 23 – 25 show the comparison between *htc* distributions for different rib configurations. These figures show that the CFD is unable to predict the levels of the heat transfer coefficient for both ribs and surfaces between the ribs. Also it fails to predict the *htc* pattern observed in the passage upstream of the first hole. The reason for this is that in the experimental tests there was a smooth bell mouth intake and heater mesh combination that was not modelled in the CFD simulations (a right-angle edge entry was used instead). The CFD trend that indicates a higher heat transfer coefficient at the inlet of the passage, which then drops before the flow encounters any features in the passage, is consistent with Boelter et al. [16].

Figure 26 shows the comparison of *htc* distributions between experimental and computational models for the case with no ribs. Experimental data suggests that a vortex is being set up radially at the position of the first hole on the bottom side of the passage, and the remaining flow is strongly affected by this. This is observed in both surfaces (hole surface and opposite surface), although it is more visible on the opposite to the holes surface. CFD is unable to predict this phenomenon.

Experimental data show that the flow re-attaches downstream of the hole much quicker than the CFD prediction. For the first 10 holes the flow re-attaches at a distance equal to about 2/5 of the hole pitch compared to 1 hole pitch for the CFD simulation. For the remaining of the holes the situation is reversed. In the experiments the flow re-attaches at about half a hole pitch whereas in the CFD the enhancement steadily declines. The stripping of the boundary layer immediately downstream of the hole is much stronger in the experimental data, especially from hole 7 onwards.

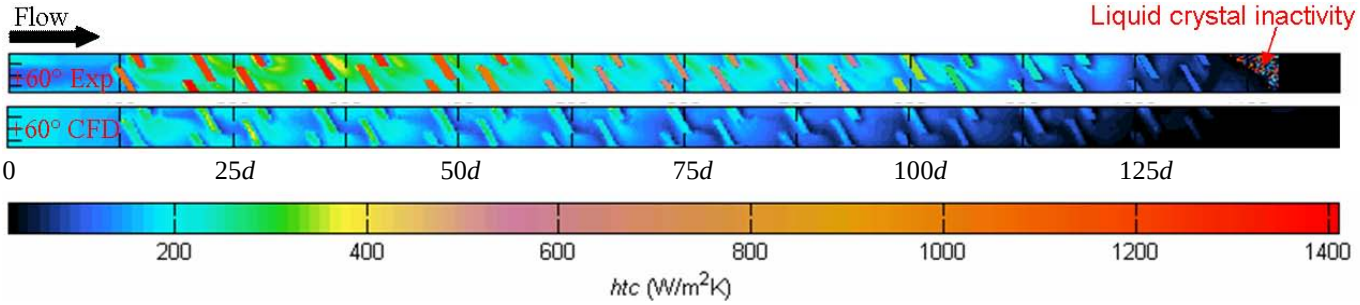

Figure 23 – Comparison of *htc* distributions for the +60º configuration, Re_{inlet} = 69959

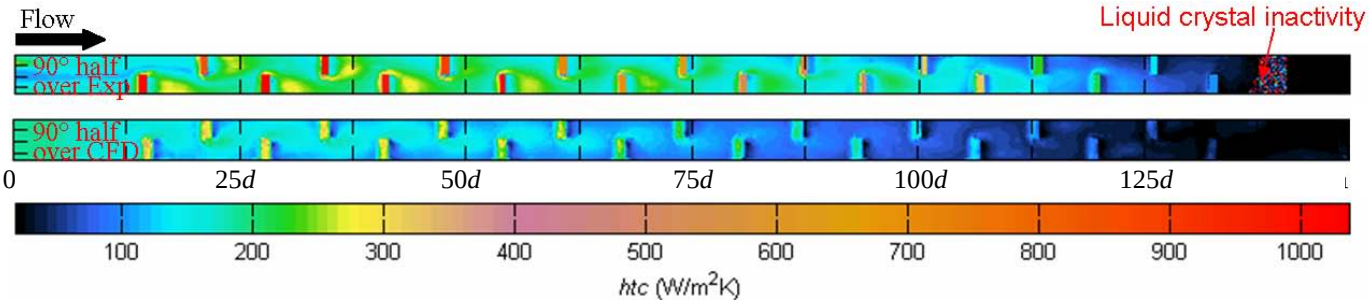

Figure 24 – Comparison of *htc* distributions for the 90º half ribs, over hole configuration, Re_{inlet} = 69959

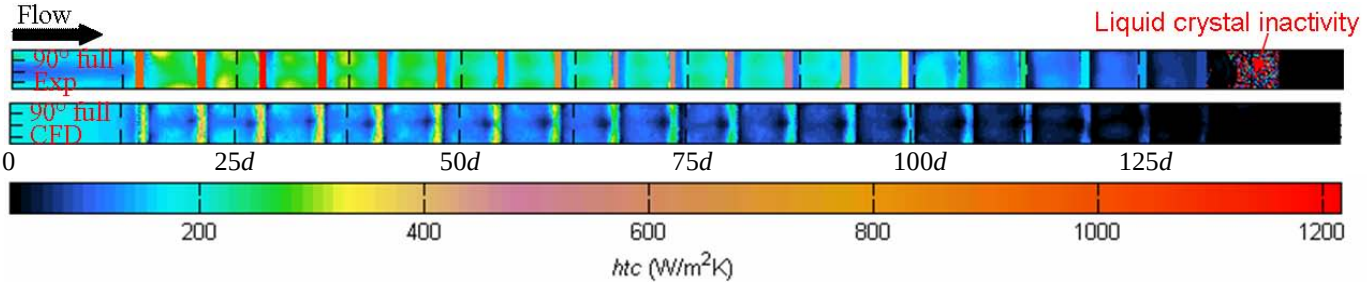

Figure 25 – Comparison of *htc* distributions for the 90º full ribs configuration, Re_{inlet} = 69959

Passage total pressure drop

The penalty for adding flow turbulators to the cooling passage is, of course additional pressure drop along it. Figure 27 shows the total pressure drop in the passage at Re_{inlet} = 69959 determined both experimentally and computationally. The figure clearly shows that the highest total pressure drop is not associated with the one with the highest *htc* enhancement. The +60º rib configuration has 6 % higher *htc* enhancement than the 90º full ribs but 10% lower total passage pressure drop. The lowest total pressure drop occurs for the 90º half ribs, over hole configuration but this also had the lowest experimentally measured *htc* enhancement. Since passage total pressure drop values scale proportionately to average friction factor values, a second axis has been added to Figure 27 to show equivalent average friction factors. The final value shows the Blasius value adjusted for a smooth pipe with flow extraction. The results show that the experimental smooth passage average friction factor is 1.7 × the Blasius friction factor, while in the ribbed passage this is up to ~9 × higher in the case of 90° full ribs.

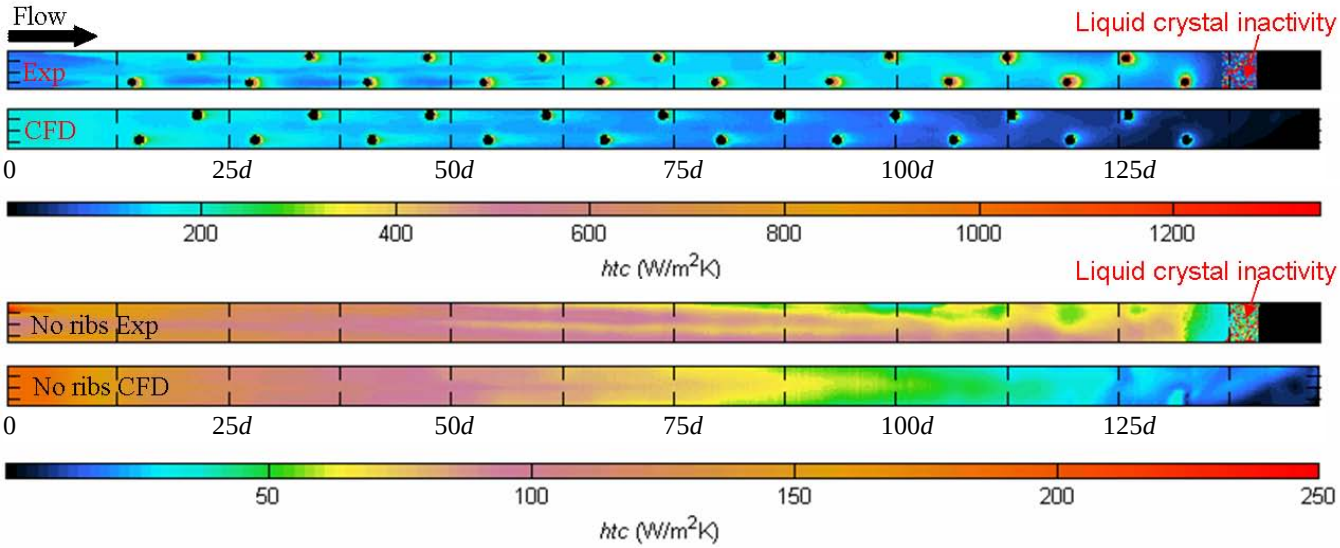

Figure 26 – Comparison of *htc* distributions for case with no ribs, Re_{inlet} = 69959

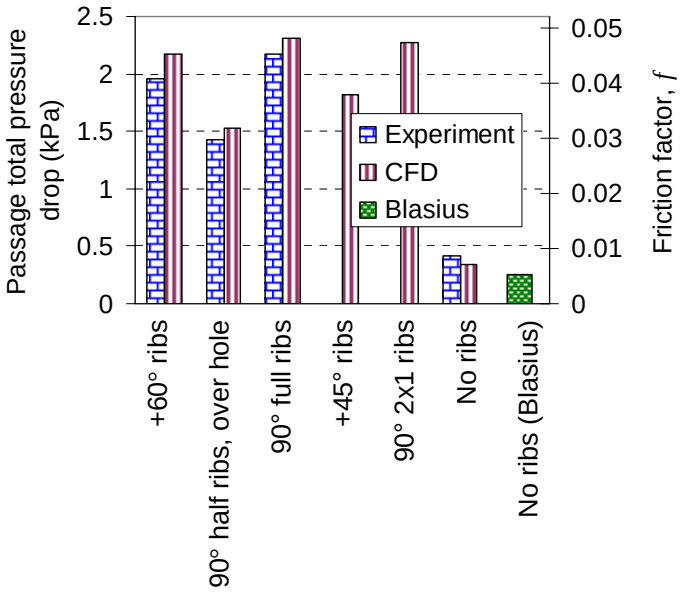

Figure 27 – Experimental and CFD comparison for passage total pressure drop

The CFD predictions of total pressure drop are close to those measured experimentally. Changing the orientation of the 60º, 45º and 90º half ribs make very little difference to the total pressure drop. Interestingly the CFD *htc* predictions show the 45º configuration to have equivalent or higher *htc* enhancement than the 60º ribs but with lower associated total pressure drop.

EXPERIMENTAL AND COMPUTATIONAL UNCERTAINTIES

Experimental Uncertainty

Uncertainty analysis was carried out using the method outlined by Moffat [17]. This shows that the root sum square error in the heat transfer coefficient measurements is between 6.00 and 6.03 % depending on the heat transfer coefficient level, and in the worst case this rises to between 10.43 and 11.62%. Table 2 shows the uncertainty ascribed to each measurand and the results of the uncertainty analysis. Values in **bold** refer to the uncertainty for the copper ribs *htc* calculation.

Grid sensitivity

To test for grid sensitivity two additional computational meshes were generated. In the first of these the number of cells was halved to 1.15×10^6, however the boundary layer was unaltered to maintain the required condition of $y^+ \leq 1$ in wall adjacent cells. Figure 28 shows a maximum variation of 0.044 % between the two CFD grids and an error of 0.7 % between the experimental measurements and the 2.3×10^6 cells grid converged solution. In the second mesh the boundary layer was resolved such that maximum $y^+ = 0.1$ in wall adjacent cells. Only the initial two transfer holes could be modelled at this resolution because of computational limitations. As the flow is highly parabolic, this was not of concern. Passage and hole mass flow rate boundary conditions were used to model the flow in the first two holes. Maximum and average variation of 0.55 % and 1.79 % respectively were found between these heat transfer coefficients, and those predicted using the 2.3×10^6 cell grid.

Parameters	Typical values	Typical Error	Low *htc* error	High *htc* error
$T_{initial}$ (ºC)	17.3	0.3	1.14 %	1.01 %
			2.21 %	**1.69 %**
T_{gas} (ºC)	67.0	0.3	1.44 %	1.88 %
			2.21 %	**1.69 %**
$T_{crystal}$ (ºC)	39.9	0.3	2.61 %	2.87 %
			2.21 %	**1.69 %**
$t_{crystal}$ (s)	14.9	0.04	0.17 %	1.13 %
			0 %	**0.68 %**
$\sqrt{\rho ck}$	569	29	5.07 %	4.71 %
			0.74 %	**0.51 %**
Mass of copper rib (g)	**6.3**	**0.1**	**1.47 %**	**1.35 %**
Base value of *htc* (W/m^{2}K)	-	-	143	417
			136	**1182**
Liquid crystal RSS error			6.00 %	6.03 %
Liquid crystal Worst case			10.43 %	11.62 %
Copper rib RSS error			**4.16 %**	**3.34 %**
Copper rib Worst case			**8.82 %**	**7.61 %**

Table 2 – Uncertainty analysis for heat transfer coefficient measurements

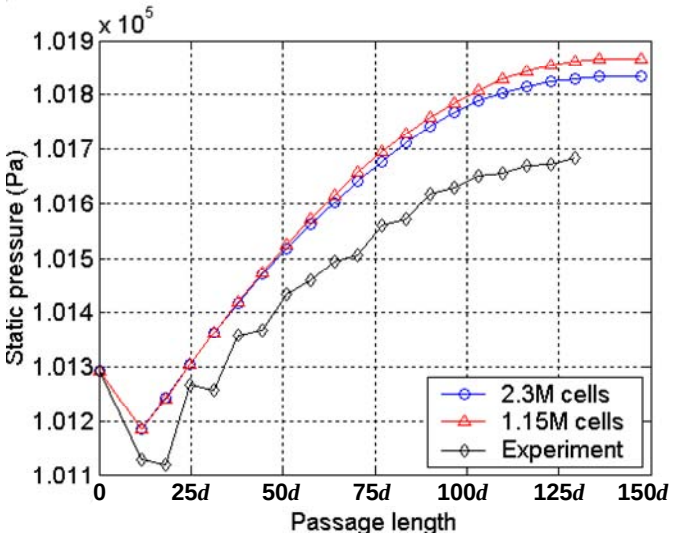

Figure 28 – Passage static pressure

SUMMARY AND CONCLUSION

An experimental and computational series of tests were carried out to investigate the effect of turbulators on the heat transfer coefficient of a cooling manifold. The experimental data obtained indicate that different rib configurations provide different levels of *htc* enhancement on the ribbed wall and total pressure drop along the cooling passage.

From the configurations tested and for Re_{inlet} = 69959, the +60° ribs provide a combined (ribs and surface between ribs) *htc* enhancement of 60 % on the ribbed wall with an associated total pressure drop which is 78 % higher compared to the case with no

ribs. The percentages for the 90° full ribs are 56 % and 81 % and for the 90° half ribs, over hole, are 46 % and 70 % respectively.

A computational study, in which the *htc* enhancement on the holed surface was also investigated, showed that it is possible, with the right selection of rib configuration, to maximise the *htc* on the ribbed or the holed surface. Computational results agree qualitatively with experimental data. The 90° full ribs provide the highest *htc* enhancement for the holed surface with a 22 % increase over the case with no ribs. For the ribbed wall the highest combined *htc* enhancement is provided by the $\pm 45°$ ribs followed closely by the $\pm 60°$ ribs. Considering *htc* enhancement over both surfaces and total pressure drop across the manifold passage, computational results show that $\pm 45°$ ribs perform better.

ACKNOWLEDGMENTS

This work has been carried out with the support of Rolls-Royce plc. The experimental apparatus was manufactured by Mr. Pat Timms and Mr. Nigel Brett.

REFERENCES

[1] Ieronymidis, I., Gillespie, D.R.H., Ireland, P.T, and Kingston, R., 2006, "Detailed Heat Transfer Measurements in a Model of an Integrally Cast Cooling Passage", ASME Paper No. GT2006-91231, Turbo Expo 2006: Power for Land, Sea & Air, May 8 – 11, Barcelona, Spain.

[2] Berger, F.P., Hau, F.L., and Hau, K.F., 1979, "Local Mass/Heat Transfer Distribution on Surfaces Roughened with Small Square Ribs", International Journal of Heat and Mass Transfer, Vol. 22, pp. 1645-1656.

[3] Metzger, D.E., Chyu, M.K., and Bunker, R.S., 1988, "The Contribution of on Rib Heat Transfer Coefficients to Total Heat Transfer from Rib Toughened Surfaces, Transport Phenomena in Rotating Machinery", Published by Hemisphere Publishing Co.

[4] Taslim, M.E., and Wadsworth, C.E., 1994, "An Experimental Investigation of the Rib Surface-Averaged Heat Transfer Coefficient in a Rib-Roughened Square Passage", ASME Paper No. 94-GT-162.

[5] Korotky, G.J., and Taslim, M.E., 1998, "Rib Heat Transfer Coefficient Measurements in a Rib-Roughened Square Passage", ASME Journal of Turbomachinery, Vol. 120, pp. 376-385.

[6] Hermanson, K., Parneix, S., Von Wolfersdorf, J., and Semmler, K., 2001, "Prediction of Pressure Loss and Heat Transfer in Internal Cooling Passages", Annals of the New York Academy of Sciences, Vol. 934, pp. 448-455.

[7] Hwang, G.J., Tzeng, S.C., Mao, C.P., and Soong, C.Y., 2001, "Heat Transfer in a Radially Rotating Four-Pass Serpentine Channel With Staggered Half-V Rib Turbulators", Journal of Heat Transfer, Vol. 123, pp. 39-50.

[8] Tsang, C.L.P., Gillespie, D.R.H., and Ireland, P.T., 2005, "Flow measurements inside a large scale model of a turbine component internal cooling passage", Proceedings 6th European Conference on Turbomachinery, Fluid Dynamics and Thermodynamics, 7-11 March, Lille, France.

[9] Andrews, G.E. and Mkpadi, M.C., 1983, "Full Coverage Discrete Hole Wall Cooling: Discharge Coefficients", ASME Paper No. 83-GT-79, International Gas Turbine Conference and Exhibit, Phoenix, Arizona, March 1983.

[10] Abu Talib, A.R., Ireland, P.T., Neely, A.J., and Mullender, A.J., 2003, "A Novel Liquid Crystal Image Processing Technique using Multiple Gas Temperature Tests to Determine Heat Transfer Coefficient Distribution and Adiabatic Wall Temperature", ASME paper No. GT2003-38198.

[11] Schultz, D.L., and Jones, T.V., 1973, "Heat Transfer Measurements in Short Duration Hypersonic Facilities", AGARDograph No. 165.

[12] Wang, Z., Ireland P.T., Jones T.V., 1991, "A Technique for Measuring Convective Heat Transfer at Rough Surfaces", ASME paper No. 90-GT-300.

[13] Fluent manual, 2003, Fluent Inc.

[14] Tsang, C.L.P., 2002, "High Blockage Turbulators in Gas Turbine Cooling Passages", D.Phil. Thesis, Department of Engineering Science, University of Oxford.

[15] Han, J.C., Zhang, Y.M., and Lee, C.P., 1991,"Augmented Heat Transfer in Square Channels with Parallel, Crossed and V-shaped Angled Ribs," Journal of Heat Transfer, Vol. 113, pp. 590-596.

[16] Boelter, L.M.K., Young, G., and Iverson, H.W., 1945, "An Investigation of Aircraft Heaters. XXVII – Distribution of Heat Transfer Rate in the Entrance Section of a Circular Tube, NACA TN 1451.

[17] Moffat, R.J., 1988, "Describing the Uncertainties in Experimental Results", Experimental Thermal and Fluid Science, Vol. 1, pp. 3-17.